

Denoising Diffusion Probabilistic Models for Coastal Inundation Forecasting

Kazi Ashik Islam¹, Zakaria Mehrab¹, Mahantesh Halappanavar², Henning Mortveit¹, Sridhar Katragadda³, Jon Derek Loftis⁴ and Madhav Marathe¹

¹Biocomplexity Institute, University of Virginia

²Pacific Northwest National Laboratory

³Department of Communications and Information Technology, City of Virginia Beach

⁴Virginia Institute of Marine Science, College of William and Mary

{ki5hd, zm8bh}@virginia.edu, hala@pnnl.gov, Henning.Mortveit@virginia.edu, SKatraga@vbgov.com, jdloftis@vims.edu, marathe@virginia.edu

Abstract

Coastal flooding poses significant risks to communities, necessitating fast and accurate forecasting methods to mitigate potential damage. To approach this problem, we present DIFF-FLOOD, a probabilistic spatiotemporal forecasting method designed based on denoising diffusion models. DIFF-FLOOD predicts inundation level at a location by taking both spatial and temporal context into account. It utilizes inundation levels at neighboring locations and digital elevation data as spatial context. Inundation history from a context time window, together with additional co-variates are used as temporal context. Convolutional neural networks and cross-attention mechanism are then employed to capture the spatiotemporal dynamics in the data. We trained and tested DIFF-FLOOD on coastal inundation data from the Eastern Shore of Virginia, a region highly impacted by coastal flooding. Our results show that, DIFF-FLOOD outperforms existing forecasting methods in terms of prediction performance (6% to 64% improvement in terms of two performance metrics) and scalability.

1 Introduction

The projection in sea level rise have highlighted the increasing vulnerability of many coastal regions to inundation [Wuebbles *et al.*, 2017]. Among these regions, the East Coast in US is a region of particular policy concern due to its geography and low-lying topography [Ezer and Atkinson, 2014]. This region, in recent periods, has been experiencing frequent inundation events [Ezer, 2020], causing disruptions in daily life (e.g. traffic, economic) [Jacobs *et al.*, 2018]. In the future, this situation will only keep declining due to the combined effect of climate change, sea level rise, and urbanization [Swain *et al.*, 2020]. Therefore, forecasting coastal inundation is of utmost importance from a policy standpoint for undertaking risk prevention measurement or safe evacuation of the residents in danger [Yang *et al.*, 2019].

The problem of coastal inundation forecasting came to our attention during conversations with staff at the City of Vir-



Figure 1: Flooding on Quinby Bridge Road, Accomack County, VA on April 3, 2024 (Data source: Tidewatch Maps [Tidewatch, 2025].)

ginia Beach. The region faces challenges with coastal flooding which causes slow-down and/or road closures; disrupting the day-to-day activities of the inhabitants. A fast and high-resolution flood forecasting model would enable city officials to identify localized inundation model risks, resulting in more effective preparedness and response. In this paper, we approach the problem of designing such a model. It is a joint-work of a multidisciplinary team, including computer and data scientists, academic experts with expertise in hydro-dynamic models, members of established coastal resources management centers, and officials at the City of Virginia Beach.

The traditional method for predicting inundation involves hydro-dynamical, physics-based models (PBM). Commercially available [Syme, 2001; Deltares, 2014] (e.g., SOBEK, TUFLOW) or open-sourced [Zhang *et al.*, 2016] (e.g., SCHISM) hydro-dynamical models can simulate inundation accurately at a high resolution. However, the computation time associated with these PBMs makes them challenging for real-time forecasting [Guo and others, 2021]. Although researchers have investigated Deep-Learning (DL) based time-series prediction methods as surrogates to these PBMs [Roy *et al.*, 2023], these models are not suitable for accommodating spatial contexts. Existing spatiotemporal forecast-

ing methods, on the other hand, struggle to scale in high-resolution forecasting tasks.

Motivated by the above observations, we explore the Diffusion Model [Sohl-Dickstein *et al.*, 2015] in the context of high-resolution coastal inundation forecasting task. The primary reason for investigating diffusion models is its ability to utilize conditioning contexts of various dimensions [Romach *et al.*, 2022; Zhang and others, 2023] and its potential to model physical properties [Ahmad and others, 2024; Amram and Pedro, 2023]. Originally developed for image generation, diffusion models have been adapted for time-series forecasting, achieving state-of-the-art performance, as demonstrated by Rasul *et al.* (2021). However, their approach does not incorporate spatial context. More recently, [Wen *et al.*, 2023] proposed a probabilistic spatiotemporal graph forecasting method based on denoising diffusion models. While promising, such methods face scalability challenges when applied to large-scale/high-resolution inundation forecasting tasks. Using the coastal inundation of the Eastern Shore as case study, we address these challenges by making the following contributions in this paper.

- We formulate the problem of coastal inundation forecasting under the spatiotemporal forecasting framework and introduce DIFF-FLOOD as a novel method for approaching the problem. It can utilize both spatial and temporal context to generate spatiotemporal forecasts at fine spatial resolution.
- Extensive evaluation of our method against several baseline methods on inundation data of the Virginia Eastern Shore underscores the superiority of our proposed method and its aspect of being used as a decision-making tool for policymakers. Specifically, we observed 6% to 64% improvement in prediction performance, in terms of two performance metrics (Normalized Average Continuous Ranked Probability Score, and Normalized Root Mean Square Error). An ablation study of our model is performed to highlight the importance of its components.
- Furthermore, we demonstrate the scalability of our model compared to other baselines in large settings, underscoring its utility in real-time forecasting in large-scale scenarios.

It is worth highlighting that our model can be used to answer inundation scenario-based queries relevant to policymakers. For example, queries of the form: “*What is the probability that a particular region will get inundated by 1 feet within the next 12 hours?*”, can be answered by using our model through probabilistic forecasting, see section 7.

2 Related Work

We present an abridged version of the most relevant literature in this section. The supplementary material of this paper covers the literature more extensively.

Hydrology Models: Traditionally, various Physics Based hydrodynamic Models (PBM) have been employed to simulate inundation. SOBEK [Deltares, 2014] is a 2D model that solves a Saint-Venant flow equation and shallow water equation to determine the water level of rectangular grids. TELEMAC-2D [Vu *et al.*, 2015] uses a similar method but is more suitable for coastal areas. Polymorphic models like

SCHISM [Zhang *et al.*, 2016] can capture water flow at very high resolution. However, the computation time associated with solving these complex equations at high spatial resolution makes these PBMs infeasible for real-time forecasting.

Deep Learning: DL methods are a popular choice in surrogating hydrodynamic models. Regression-based methods [Zahura and Goodall, 2022], recurrent neural networks [Roy *et al.*, 2023] and hybrid ML-based methods [Zanchetta and Coulibaly, 2022] are some of the methods that have been attempted as possible surrogates. However, these models cannot inherently take spatial context into account. The DCRNN method proposed by [Li *et al.*, 2017] for traffic forecasting is the state-of-the-art DL method for spatiotemporal point forecasting, where bidirectional random walk is used to capture spatial dependency and Seq2Seq architecture is used to capture temporal dependency.

Diffusion Model The field of generative modeling has been dominated by the diffusion model for quite some time. Although it had primarily been studied for image synthesis [Ho *et al.*, 2020; Dhariwal and Nichol, 2021; Austin *et al.*, 2021], its fascinating ability to use flexible conditioning to guide the generation process has been utilized in other domains like video generation [Yang *et al.*, 2023b], prompt-based image generation [Ramesh *et al.*, 2022], text-to-speech generation [Yang *et al.*, 2023a]. TimeGrad [Rasul *et al.*, 2021] was the pioneering method that approached the time-series forecasting problem by utilizing a diffusion model. Other models like CSDI [Tashiro *et al.*, 2021], DPSD-CSPD [Biloš *et al.*, 2023], TDSTF [Chang *et al.*, 2024] were later introduced. These models try to predict the noise added during the forward process of the diffusion model (ϵ -parameterization). An alternative parameterization is to predict the ground-truth data (x -parameterization). Different from models mentioned above, D^3 VAE [Li *et al.*, 2022] uses coupled diffusion process and bidirectional variational autoencoder to better forecast in longer horizon and improve interpretability. The State-of-the-Art Diffusion-based model DiffSTG [Wen *et al.*, 2023] devised a modified architecture for the reverse process of diffusion model combining UNet and GNN to capture temporal and spatial dependencies, respectively. However, both these methods scale poorly with the growth in number of variables.

3 Problem Formulation

Formally, we define the inundation forecasting problem as follows.

Problem 1. Single Patch Probabilistic Inundation Forecasting. Let P denote a two-dimensional rectangular grid of size $D \times D$, henceforth called a ‘patch’. Let $\mathbf{x}_t^0 \in \mathbb{R}^{D \times D}$ denote the inundation matrix of patch P at timestep t , where $x_{ij,t}^0 \in \mathbb{R}$ denotes the inundation level on cell (i, j) of patch P at time step t ; $i, j \in \{1, \dots, D\}, t \in \{1, \dots, T\}$. Let $\mathbf{s} \in \mathbb{R}^{D \times D}$ denote the elevation matrix of patch P , where s_{ij} denotes the elevation of cell (i, j) . Let $\mathbf{z}_t \in \mathbb{R}^l, t \in \{1, \dots, T\}$ denote a time series of co-variables associated with patch P . Let $t_0 : t_{c+l}$ denote the increasing sequence of timesteps t_0, t_1, \dots, t_{c+l} , where $c, l > 0$. We aim to learn the conditional distribution function $q(\mathbf{x}_{t_c:t_{c+l}}^0 | \mathbf{x}_{t_0:t_{c-1}}^0, \mathbf{z}_{t_0:t_{c-1}}, \mathbf{s})$.

Problem 2. Multi-patch Probabilistic Inundation Forecasting Let $\mathcal{P} = \{P_1, P_2, \dots, P_K\}$ denote a set of dimensional patches of size $D \times D$. Let ${}_k \mathbf{x}_t^0 \in \mathbb{R}^{D \times D}$ denote the inundation matrix of patch P_k at timestep $t \in \{1, \dots, T\}$. Let ${}_k \mathbf{s} \in \mathbb{R}^{D \times D}$ and ${}_k \mathbf{z}_t \in \mathbb{R}^l, t \in \{1, \dots, T\}$ denote the elevation matrix and time series of co-variables associated with patch P_k , respectively. Let $t_0 : t_{c+l}$ denote the increasing sequence of timesteps t_0, t_1, \dots, t_{c+l} , where $c, l > 0$. We aim to learn the conditional distribution function $q({}_k \mathbf{x}_{t_c:t_{c+l}}^0 | {}_k \mathbf{x}_{t_0:t_{c-1}}^0, {}_k \mathbf{z}_t, {}_k \mathbf{s})$.

Note that, both problems are spatio-temporal forecasting problems, since we aim to forecast the inundation level on all cells in a patch together. They are also probabilistic forecasting problems, as we want to learn the distribution of inundation values instead of making a single prediction. Finally, Problem 2 represents a generalized version of Problem 1. Here, we aim to learn a single model that can be utilized to forecast inundation levels on multiple patches/areas.

The following section presents the basics of a denoising diffusion model used by our method DIFF-FLOOD for learning our target distributions. Subsequently, we present details on how we have designed DIFF-FLOOD to capture spatial and temporal dynamics of our inundation values.

4 Denoising Diffusion Model

In this section, we provide a brief overview of denoising diffusion models. A more comprehensive view is provided in the supplementary material.

Let $\mathbf{x}^0 \sim q_\chi(\mathbf{x}^0)$ denote the multivariate training vector from some input space $\chi = \mathbb{R}^D$, where $q_\chi(\mathbf{x}^0)$ denotes the true distribution. In diffusion probabilistic models, we aim to approximate $q_\chi(\mathbf{x}^0)$ by a probability density function $p_\theta(\mathbf{x}^0)$ where θ denotes the set of trainable parameters. Diffusion probabilistic models [Sohl-Dickstein *et al.*, 2015; Luo, 2022] are a special class of Hierarchical Variational Autoencoders [Kingma *et al.*, 2016; Sønderby *et al.*, 2016] with the form $p_\theta(\mathbf{x}^0) = \int p_\theta(\mathbf{x}^{0:N}) d\mathbf{x}^{1:N}$; here $\mathbf{x}^1, \mathbf{x}^2, \dots, \mathbf{x}^N$ are latent variables. Three key properties of diffusion models are: (i) all of the latent variables are assumed to have the dimension D as \mathbf{x}^0 , (ii) the approximate posterior,

$$q(\mathbf{x}^{1:N} | \mathbf{x}^0) = \prod_{n=1}^N q(\mathbf{x}^n | \mathbf{x}^{n-1})$$

is fixed to a Markov chain (often referred to as the *forward process*), and (iii) the structure of the latent encoder at each hierarchical step is pre-defined as a linear Gaussian model as follows:

$$q(\mathbf{x}^n | \mathbf{x}^{n-1}) = \mathcal{N}(\mathbf{x}^n; \sqrt{1 - \beta_n} \mathbf{x}^{n-1}, \beta_n \mathbf{I}).$$

Additionally, the Gaussian parameters $(\beta_1, \beta_2, \dots, \beta_n)$ are chosen in such a way that we have: $q(\mathbf{x}^N) = \mathcal{N}(\mathbf{x}^N; \mathbf{0}, \mathbf{I})$.

The joint distribution $p_\theta(\mathbf{x}^{0:N})$ is called the reverse process. It is defined as a Markov chain with learned Gaussian transitions beginning at $p(\mathbf{x}^N)$:

$$p_\theta(\mathbf{x}^{0:N}) = p(\mathbf{x}^N) \prod_{n=1}^N p_\theta(\mathbf{x}^{n-1} | \mathbf{x}^n)$$

Each subsequent transition is parameterized as follows:

$$p_\theta(\mathbf{x}^{n-1} | \mathbf{x}^n) = \mathcal{N}(\mathbf{x}^{n-1}; \mu_\theta(\mathbf{x}^n, n), \Sigma_\theta(\mathbf{x}^n, n) \mathbf{I}) \quad (1)$$

Both $\mu_\theta : \mathbb{R}^D \times \mathbb{N} \rightarrow \mathbb{R}^D$ and $\Sigma_\theta : \mathbb{R}^D \times \mathbb{N} \rightarrow \mathbb{R}^+$ take two inputs: $\mathbf{x}^n \in \mathbb{R}^D$ and the noise step $n \in \mathbb{N}$. The parameters θ are learned by fitting the model to the data distribution $q_\chi(\mathbf{x}^0)$. This is done by minimizing the negative log-likelihood via a variational bound:

$$\begin{aligned} \log p_\theta(\mathbf{x}^0) &= \log \int p_\theta(\mathbf{x}^{0:N}) d\mathbf{x}^{1:N} \\ &= \log \mathbb{E}_{q(\mathbf{x}^{1:N} | \mathbf{x}^0)} \frac{p_\theta(\mathbf{x}^{0:N})}{q(\mathbf{x}^{1:N} | \mathbf{x}^0)} \\ &\geq \mathbb{E}_{q(\mathbf{x}^{1:N} | \mathbf{x}^0)} \log \frac{p_\theta(\mathbf{x}^{0:N})}{q(\mathbf{x}^{1:N} | \mathbf{x}^0)} \end{aligned} \quad (2)$$

$$\implies -\log p_\theta(\mathbf{x}^0) \leq \mathbb{E}_{q(\mathbf{x}^{1:N} | \mathbf{x}^0)} \log \frac{q(\mathbf{x}^{1:N} | \mathbf{x}^0)}{p_\theta(\mathbf{x}^{0:N})} \quad (3)$$

Here, we get (2) by applying Jensen's inequality. We indirectly minimize the negative log-likelihood of the data, i.e., $-\log p_\theta(\mathbf{x}^0)$, by minimizing the right hand side of (3).

Ho *et al.* [2020] showed that the forward process has the following property: we can sample \mathbf{x}^n using \mathbf{x}^0 at any noise step n in closed form. Let, $\alpha_n = 1 - \beta_n$, and $\bar{\alpha}_n = \prod_{i=1}^n \alpha_i$. Then, we have:

$$q(\mathbf{x}^n | \mathbf{x}^0) = \mathcal{N}(\mathbf{x}^n; \sqrt{\bar{\alpha}_n} \mathbf{x}^0, (1 - \bar{\alpha}_n) \mathbf{I}). \quad (4)$$

Based on this property, Ho *et al.* [2020] showed that one possible parameterization of (1) is as follows:

$$\mu_\theta(\mathbf{x}^n, n) = \frac{\sqrt{\bar{\alpha}_n}(1 - \bar{\alpha}_{n-1})}{1 - \bar{\alpha}_n} \mathbf{x}^n + \frac{\sqrt{\bar{\alpha}_{n-1}} \beta_n}{1 - \bar{\alpha}_n} \hat{\mathbf{x}}_\theta(\mathbf{x}^n, n) \quad (5)$$

$$\Sigma_\theta(\mathbf{x}^n, n) = \frac{1 - \bar{\alpha}_{n-1}}{1 - \bar{\alpha}_n} \beta_n \quad (6)$$

Here, $\hat{\mathbf{x}}_\theta(\mathbf{x}^n, n)$ is a neural network that predicts \mathbf{x}^0 from noisy vector \mathbf{x}^n and noise step n . Ho *et al.* [2020] then showed that, the right hand side of (3) can be minimized by minimizing:

$$\mathbb{E}_{\mathbf{x}^n, q(\mathbf{x}^n | \mathbf{x}^0)} \frac{1}{2\tilde{\beta}_n} \frac{\bar{\alpha}_{n-1} \beta_n^2}{(1 - \bar{\alpha}_n)^2} \|\mathbf{x}^0 - \hat{\mathbf{x}}_\theta(\mathbf{x}^n, n)\|_2^2 \quad (7)$$

Therefore, optimizing a diffusion model can be done by training a neural network to predict the original ground truth vector from an arbitrarily noisy version of it. Once trained, to sample from the reverse process $\mathbf{x}^{n-1} \sim p_\theta(\mathbf{x}^{n-1} | \mathbf{x}^n)$, we first sample \mathbf{x}^N from $\mathcal{N}(\mathbf{0}, \mathbf{I})$. Then, we compute:

$$\mathbf{x}^{n-1} = \mu_\theta(\mathbf{x}^n, n) + \sqrt{\Sigma_\theta} \mathbf{v} \quad (8)$$

Here, $\mathbf{v} \sim \mathcal{N}(\mathbf{0}, \mathbf{I})$ for $n \in [2, N]$, and $\mathbf{v} = \mathbf{0}$ when $n = 1$. $\mu_\theta(\mathbf{x}^n, n)$ and Σ_θ are computed using (5) and (6), respectively.

5 DIFF-FLOOD Method

DIFF-FLOOD is designed for multi-patch probabilistic inundation forecasting, where the inundation values are correlated both spatially and temporally. Following our notations in Problem 1 and 2, let ${}_k \mathbf{x}_t^0 \in \mathbb{R}^{D \times D}$ denote

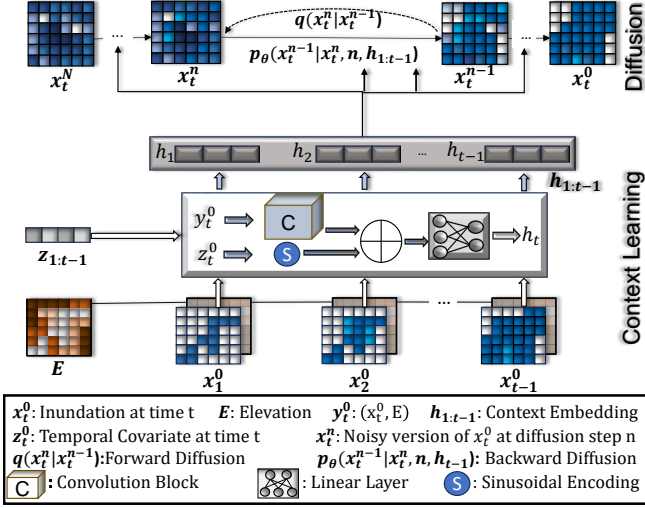


Figure 2: Architecture of proposed DIFF-FLOOD Model

the inundation matrix of the patch P_k at time step t . Towards our goal of learning the conditional distribution $q_\chi(k\mathbf{x}_{t_c:t_{c+1}}^0 | k\mathbf{x}_{t_0:t_{c-1}}^0, k\mathbf{z}_{t_0:t_{c-1}}, k\mathbf{s})$, where $k\mathbf{s} \in \mathbb{R}^{D \times D}$ is the elevation matrix of patch P_k , and $k\mathbf{z}_t$ denotes a time-series of co-variables associated with P_k , we assume:

$$q_\chi(k\mathbf{x}_{t_c:t_{c+1}}^0 | k\mathbf{x}_{t_0:t_{c-1}}^0, k\mathbf{z}_{t_0:t_{c-1}}, k\mathbf{s}) = \prod_{t=t_c}^{t_{c+1}} q_\chi(k\mathbf{x}_t^0 | k\mathbf{x}_{t_0:t-1}^0, k\mathbf{z}_{t_0:t-1}, k\mathbf{s}) \quad (9)$$

In DIFF-FLOOD, we use a denoising diffusion model (as described in Section B) to learn the conditional distributions on the right hand side of (9). We refer to $k\mathbf{x}_{t_0:t-1}^0$, $k\mathbf{z}_{t_0:t-1}$, and $k\mathbf{s}$ as *context* data.

To capture spatial correlation, we first augment the inundation data in the context (i.e. $k\mathbf{x}_{t_0:t-1}^0$) by concatenating the elevation matrix $k\mathbf{s}$ to it as an additional channel (Equation 10). The goal is to capture the correlation of elevation and inundation values. We then use convolution blocks extract spatial features $k\mathbf{f}_{t_0:t-1}$ (Equation 11).

$$k\mathbf{y}_{t_0:t-1}^0 = k\mathbf{x}_{t_0:t-1}^0 \oplus k\mathbf{s} \quad (10)$$

$$k\mathbf{f}_{t_0:t-1} = \text{CONV}_{\theta_1}(k\mathbf{y}_{t_0:t-1}^0) \quad (11)$$

In addition, since coastal inundation is expected to be correlated with tide cycles, we use the hour of day, and day of month as temporal features \mathbf{z}_t . We use sinusoidal encoding to capture the cyclic nature of these temporal features.

$$k\mathbf{g}_{t_0:t-1}^0 = \text{SINUSOID}(k\mathbf{z}_{t_0:t-1}) \quad (12)$$

We concatenate the spatial and temporal features, and then pass it through a linear fully connected layer to get an embedding of the context.

$$k\mathbf{h}_{t_0:t-1} = \text{LINEAR}_{\theta_2}(k\mathbf{f}_{t_0:t-1} \oplus k\mathbf{g}_{t_0:t-1}^0) \quad (13)$$

An overview of the architecture of DIFF-FLOOD is provided in Figure 2. We approximate (9) by the model in (14). Here, θ comprises of the trainable parameters of the convolution blocks (θ_1), fully connected layer (θ_2), and the denoising diffusion model (θ_3).

$$\prod_{t=t_c}^{t_{c+1}} p_\theta(k\mathbf{x}_t^0 | k\mathbf{h}_{t_0:t-1}) \quad (14)$$

Algorithm 1: Training for patch P_k , prediction time step t

Input: Data: $k\mathbf{x}_t^0 \sim q(k\mathbf{x}_t^0)$, Context: $k\mathbf{x}_{t_0:t-1}^0$, $k\mathbf{z}_{t_0:t-1}$, $k\mathbf{s}$.

```

1 while not converged do
  // Forward diffusion
2 Initialize  $n \sim \text{Uniform}(1, N)$ .
3  $k\mathbf{x}_t^n \leftarrow \mathcal{N}(\sqrt{\alpha_n} k\mathbf{x}_t^0, (1 - \alpha_n)\mathbf{I})$ .
  // Compute context embedding
4  $k\mathbf{f}_{t_0:t-1}^0 \leftarrow \text{CONV}_{\theta_1}(k\mathbf{x}_{t_0:t-1}^0 \oplus k\mathbf{s})$ 
5  $k\mathbf{g}_{t_0:t-1}^0 \leftarrow \text{SINUSOID}(k\mathbf{z}_{t_0:t-1})$ 
   $k\mathbf{h}_{t_0:t-1} \leftarrow \text{LINEAR}_{\theta_2}(k\mathbf{f}_{t_0:t-1}^0 \oplus k\mathbf{g}_{t_0:t-1}^0)$ 
  // prediction
6  $k\hat{\mathbf{x}}_t^0 \leftarrow \hat{\mathbf{x}}_{\theta_3}(k\mathbf{x}_t^n, n, k\mathbf{h}_{t_0:t-1})$ 
7 Take gradient step on  $\nabla_{\theta} \|k\mathbf{x}_t^0 - k\hat{\mathbf{x}}_t^0\|_2^2$ 

```

As described in Section B, within the denoising diffusion model, we need to train a neural network $\hat{\mathbf{x}}_{\theta_3}(k\mathbf{x}_t^n, n, k\mathbf{h}_{t_0:t-1})$ that predicts $k\mathbf{x}_t^0$ from noisy vector $k\mathbf{x}_t^n$, noise step n , and context embedding $k\mathbf{h}_{t_0:t-1}$. We use a conditional UNet for this purpose. Within the UNet architecture, we employ a cross-attention conditioning mechanism [Rombach *et al.*, 2022] to map the context embedding to the intermediate layers of the UNet. It allows us to predict $k\mathbf{x}_t^0$ while paying attention to different parts of the context embedding.

5.1 Training

To train DIFF-FLOOD, we sample context windows ($k\mathbf{x}_{t_0:t-1}^0$) and the immediate next timestep ($k\mathbf{x}_t^0$) from the training time series data of each patch. We then optimize the parameters θ by minimizing the negative log-likelihood of the data ($-\log p_\theta(k\mathbf{x}_t^0 | k\mathbf{h}_{t_0:t-1})$). Through a similar derivation as shown in the Section B, the objective to minimize becomes:

$$\mathbb{E}_{k\mathbf{x}_t^n, n} \|k\mathbf{x}_t^0 - \hat{\mathbf{x}}_\theta(k\mathbf{x}_t^n, n, k\mathbf{h}_{t_0:t-1})\|_2^2 \quad (15)$$

Here, the neural network $\hat{\mathbf{x}}_\theta$ is now also conditioned on the context embedding $k\mathbf{h}_{t_0:t-1}$.

Algorithm 2: Sampling $k\mathbf{x}_t^0$

Input: Noise: $k\mathbf{x}_t^N \sim \mathcal{N}(\mathbf{0}, \mathbf{I})$, Context: $k\mathbf{x}_{t_0:t-1}^0$, $k\mathbf{z}_{t_0:t-1}$, $k\mathbf{s}$.

```

1 for  $n \in N, \dots, 1$  do
2   if  $n > 1$  then
3      $\mathbf{v} \sim \mathcal{N}(\mathbf{0}, \mathbf{I})$ 
4   else
5      $\mathbf{v} \leftarrow \mathbf{0}$ 
6   Compute context embedding  $k\mathbf{h}_{t_0:t-1}$ .
7    $k\hat{\mathbf{x}}_t^0 \leftarrow \hat{\mathbf{x}}_\theta(k\mathbf{x}_t^N, n, k\mathbf{h}_{t_0:t-1})$ 
8    $k\mathbf{x}_t^{n-1} \leftarrow \frac{\sqrt{\alpha_n}(1-\alpha_{n-1})}{1-\alpha_n} k\mathbf{x}_t^N + \frac{\sqrt{\alpha_{n-1}}\beta_n}{1-\alpha_n} k\hat{\mathbf{x}}_t^0$ 
9    $\phantom{k\mathbf{x}_t^{n-1}} + \sqrt{\Sigma_\theta} \mathbf{v}$ 
10 return  $k\mathbf{x}_t^0$ 

```

5.2 Inference

During inference, given a context ${}_k\mathbf{x}_{t_0:t-1}^0, {}_k\mathbf{z}_{t_0:t-1}, {}_k\mathbf{s}$, we first compute the context embedding ${}_k\mathbf{h}_{t_0:t-1}$. We then apply Algorithm 2 to obtain a sample ${}_k\mathbf{x}_t^0$ of the next time step. Based on this sample, we compute the new context embedding ${}_k\mathbf{h}_{t_0:t}$ and repeat until the desired number of prediction time steps have been reached. We repeat the process multiple times to get multiple predictions.

6 Experiment

We conduct our experiments in two parts. *First*, we evaluate DIFF-FLOOD model on the TideWatch dataset (see Section 6.1) against five competitive baseline models, taking forecasting inundation across the Virginian Eastern Shore region as our case study. *Second*, we conduct an ablation study of our model, underscoring the importance of the components of our proposed architecture.

6.1 Dataset

To train DIFF-FLOOD, we downloaded inundation data of the Eastern Shore, Virginia from Tidewatch Maps [Loftis *et al.*, 2019; Loftis, 2022]; a street-level inundation mapping tool developed by the Virginia Institute of Marine Science (VIMS). It utilizes the open-source hydro-dynamic model, SCHISM [Zhang *et al.*, 2016] as the engine, and provides 36 hour inundation forecast maps with a 12 hour update frequency. We used this dataset due to its high spatial resolution, coverage of areas affected by coastal inundation, and lack of other publicly available inundation datasets.

We downloaded 89 days (March 28, 2024 to June 24, 2024) of hourly inundation data of the area. The data comes in a raster geo-database format with a pixel resolution of $10m \times 10m$ and provides inundation level at each pixel in feet. We resampled the data to a pixel resolution of $30m \times 30m$. We then consider different square-shaped patches of size: 16×16 , 64×64 , 80×80 , and 96×96 . Each patch P_k has a time series of inundation levels denoted by ${}_k\mathbf{x}_t^0 \in \mathbb{R}^{D \times D}$, where D is the length of one side of the patch. We aim to train DIFF-FLOOD to forecast inundation levels on multiple patches.

We have used 81 days (1944 timesteps, each of length 1-hour) of data for training, 1 day (24 timesteps) of data for validation, and 7 days (168 timesteps) of data for testing. Note that, when we utilize K number of patches, the total number of both training and testing timesteps are multiplied by K . In our forecasting task, we use context window of 12 hours, and then predict the inundation levels in the subsequent 12 hours (prediction window). Each sample datapoint therefore contains 24 consecutive timesteps, first 12 hours for context and the last 12 hours for prediction. We normalize each datapoint separately as follows: first we calculate the mean and standard deviation of the inundation values in the context window, then we standardize the inundation values in both the context and prediction window using the calculated mean and standard deviation. In addition to the inundation data, we used digital elevation data [OpenTopography, 2021] for the same area. We resampled the elevation data to the same resolution of $30m \times 30m$ and then aligned it with our inundation data.

6.2 Evaluation Metric

We use two metrics to evaluate forecast quality with respect to the observations. The first metric is Normalized Root Mean Squared Error (NRMSE). Let, \mathbf{x} be the set of all observations over all cells for all timesteps. $x_{ij,t} \in \mathbf{x}$ be the observed value of cell (i, j) at time t and let, $\tilde{x}_{ij,t}$ denote the corresponding average forecast value. Then, NRMSE is defined as follows:

$$\text{NRMSE} = \frac{1}{\max_{ij,t}(\mathbf{x}) - \min_{ij,t}(\mathbf{x})} \sqrt{\frac{\sum_{ij,t} (x_{ij,t} - \tilde{x}_{ij,t})^2}{\sum_{ij,t} 1}} \quad (16)$$

In addition to NRMSE, we use an extended version of the Continuous Ranked Probability Score (CRPS) Winkler *et al.* [1996] to quantify forecast uncertainty. The CRPS metric is calculated for each cell and each timestep individually. Let’s assume that we have M forecasts $\hat{x}_{ij,t}^1, \hat{x}_{ij,t}^2, \dots, \hat{x}_{ij,t}^M$ for observation $x_{ij,t}$. *First*, the empirical cumulative distribution function (CDF) at a point z , $\hat{F}_{ij,t}^M(z)$ from these forecast values is defined as

$$\hat{F}_{ij,t}^M(z) = \frac{1}{M} \sum_{m=1}^M \mathbb{I}(\hat{x}_{ij,t}^m \leq z) \quad (17)$$

where $\mathbb{I}(y)$ is the indicator function that yields 1 if condition y holds, 0 otherwise. From this, CRPS between the empirical CDF $\hat{F}_{ij,t}^M$ and the observation $x_{ij,t}$ is calculated as

$$\text{CRPS}(\hat{F}_{ij,t}^M, x_{ij,t}) = \int_z \left(\hat{F}_{ij,t}^M(z) - \mathbb{I}(x_{ij,t} \leq z) \right)^2 dz \quad (18)$$

Since CRPS is defined for individual timestep and individual cells, we extend this metric to Normalized Average CRPS (NACRPS), defined as

$$\text{NACRPS}(\hat{F}^M, \mathbf{x}) = \frac{\sum_{ij,t} \text{CRPS}(\hat{F}_{ij,t}^M, x_{ij,t})}{\sum_{ij,t} |x_{ij,t}|} \quad (19)$$

Here, $|x_{ij,t}|$ denotes the absolute value of $x_{ij,t}$.

6.3 Baseline Comparison

In this section, we describe the baseline models compared with our model. All experiments were conducted on an HPC cluster. To achieve scalability, experiments with different configurations were conducted with the SLURM scheduler. Each job used up to 256GB CPU RAM, 8 CPU cores and could request for one GPU with maximum 40 GB GPU RAM.

1. DiffSTG [Wen *et al.*, 2023]: The State-of-the-art (SOTA) diffusion-based model for spatiotemporal forecasting.
2. TimeGrad [Rasul *et al.*, 2021] The SOTA diffusion-based model designed for Multivariate time-series forecasting.
3. DeepVAR [Salinas *et al.*, 2019]: Combines an RNN-based architecture with a Gaussian copula process output model with a low-rank covariance structure.
4. LSTNet [Lai *et al.*, 2018]: The Long-and Short-term Time-series network (LSTNet) captures local dependency pattern among variables and long-term temporal correlation among time-series trends using CNN and RNN.

Patch $D \times D \times K$	Metric	DiffSTG	DCRNN	DeepVAR	LSTNet	TimeGrad	DIFF-FLOOD
$16 \times 16 \times 2$	NACRPS	1.2523 ± 0.0445	N/A	1.4782 ± 0.0332	N/A	1.2319 ± 0.0672	0.9603 ± 0.2119 ($\uparrow 22.05\%$)
	NRMSE	<u>0.1278 ± 0.0022</u>	0.1302 ± 0.0125	0.1742 ± 0.0034	0.1439 ± 0.0003	0.1601 ± 0.0071	0.1162 ± 0.0189 ($\uparrow 9.02\%$)
$16 \times 16 \times 5$	NACRPS	1.3166 ± 0.0164	N/A	1.4151 ± 0.0293	N/A	1.2558 ± 0.0707	0.834 ± 0.1781 ($\uparrow 33.59\%$)
	NRMSE	0.1373 ± 0.0015	<u>0.1166 ± 0.0096</u>	0.1734 ± 0.0023	0.1501 ± 0.0001	0.17 ± 0.0075	0.1095 ± 0.0165 ($\uparrow 6.13\%$)
$64 \times 64 \times 10$	NACRPS	Failed	N/A	1.0228 ± 0.0895	N/A	0.5522 ± 0.0912	0.2007 ± 0.0201 ($\uparrow 63.66\%$)
	NRMSE	Failed	<u>0.0801 ± 0.0065</u>	0.3437 ± 0.035	0.1765 ± 0.0002	0.1818 ± 0.0182	0.0639 ± 0.0079 ($\uparrow 20.21\%$)
$64 \times 64 \times 20$	NACRPS	Failed	Failed	1.1451 ± 0.0792	N/A	0.545 ± 0.0181	0.227 ± 0.0249 ($\uparrow 58.34\%$)
	NRMSE	Failed	Failed	0.3967 ± 0.0419	0.1941 ± 0.0006	<u>0.1908 ± 0.0029</u>	0.0794 ± 0.008 ($\uparrow 58.39\%$)
$80 \times 80 \times 20$	NACRPS	Failed	Failed	1.1494 ± 0.1409	N/A	0.5251 ± 0.0105	0.2091 ± 0.0216 ($\uparrow 60.18\%$)
	NRMSE	Failed	Failed	0.2761 ± 0.0399	0.131 ± 0.0003	<u>0.1251 ± 0.0021</u>	0.0508 ± 0.0034 ($\uparrow 59.39\%$)
$96 \times 96 \times 20$	NACRPS	Failed	Failed	1.3578 ± 0.0372	N/A	0.5788 ± 0.016	0.2519 ± 0.0241 ($\uparrow 56.48\%$)
	NRMSE	Failed	Failed	0.1661 ± 0.0057	0.0748 ± 0.0001	<u>0.0718 ± 0.001</u>	0.0334 ± 0.0044 ($\uparrow 53.44\%$)

Table 1: Performance Comparison of DIFF-FLOOD with baseline models. All metrics are reported up to one standard deviation after conducting five experiments with different random seeds. For each configuration, the best performance is bold-highlighted and the second-best performance is underlined. For DIFF-FLOOD, percentage improvement in performance with its closest baseline competitor is shown. State-of-the-art spatiotemporal forecasting methods (e.g., DiffSTG, DCRNN) could not handle training for large patch configurations, these are marked as ‘Failed’. Since, DCRNN and LSTNet are point forecasting methods, their NACRPS metric are marked as ‘N/A’.

5. DCRNN [Li *et al.*, 2017]: A spatiotemporal forecasting framework that combines Diffusion Convolution and Sequence-to-sequence architecture to capture temporal and spatial dependencies.

Each model was trained on six different patch settings as shown in Table 1. All hyper-parameters of our model are provided in the supplementary material. It is to be noted that the number of variables increases quadratically with patch size and linearly with the number of patches. Since some models do not scale well¹ with increments in the number of variables, we limit $D = 96$ for this set of experiments. Across all experiments, we set the context and prediction length to 12. Eight scenarios were sampled to understand the quality of probabilistic forecasting. Table 1 summarizes the performance of our model with respect to the baseline models. Below, we outline some key observations from the results.

First, in terms of NACRPS, our model consistently outperforms the baselines, underscoring its superiority in probabilistic forecasting. For small patch size ($D = 16$), DIFF-FLOOD has a performance gain of between 22.05% and 33.59%, compared to its closest baseline. For larger patch sizes ($D \geq 64$), the improvement in NACRPS is close to 60%, underscoring the performance scalability of our model. Second, DIFF-FLOOD outperforms other baselines in terms of NRMSE too. Although TimeGrad was constantly the closest competitor baseline in terms of NACRPS, this is not the case here. For the smallest patch setting, DiffSTG was the best baseline in terms of NRMSE, which was outperformed by DIFF-FLOOD by 9.02%. For the next two patch settings, DCRNN was the best baseline. In these cases, DIFF-FLOOD outperformed DCRNN by 6.13% and 20.21%, respectively. For the settings with $K = 20$, DiffSTG and DCRNN both

¹It is worth mentioning we also attempted to use D^3 VAE [Li *et al.*, 2022] as a baseline. However, we it scaled poorly; causing memory error even for our lowest patch configuration.

required extensive GPU memory due to poor scalability and they failed to train. In these settings, DIFF-FLOOD outperformed TimeGrad with a margin of around 50 – 60%.

These experiments highlight that existing spatiotemporal forecasting methods (i.e., DiffSTG and DCRNN) have moderate performance but poor computation scalability, making them infeasible to deploy in large spatiotemporal settings. On the other hand, temporal forecasting methods do not have good performance scalability, making them inadequate for large-scale spatiotemporal forecasting tasks. DIFF-FLOOD has both computation and performance scalability, making it suitable for large-scale spatiotemporal forecasting tasks.

Finally, the number of parameters of the baseline models grows almost exponentially with increasing patch sizes (D), as observed from Figure 3. To investigate the reason, we analyzed the implementation of TimeGrad as an example

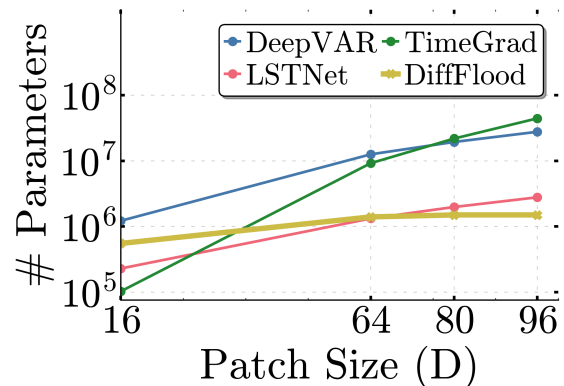


Figure 3: Scaling in Model Parameters (Log scale in Y axis) with increasing patch configuration. It has to be noted that model parameter is not affected by K . DiffSTG and DCRNN are not shown here since they fail to execute for large patch setting.

and found that it uses a fully connected layer proportional to the number of variables. On the other hand, our model utilizes a UNet architecture that creates a low-dimensional latent representation of the patches. It then performs expensive operations (e.g., feed-forward, cross-attention) on the lower-dimensional latent space, allowing it to scale quite well with the number of variables.

6.4 Ablation Study

In this section, we perform an ablation study of the DIFF-FLOOD method to investigate the effects of utilizing elevation matrix and temporal covariates, in addition to the inundation history. Specifically, given inundation history (INUN: $k\mathbf{x}_{t_0:t-1}^0$), elevation (ELEV: $k\mathbf{s}$), and temporal covariates (COV: $\mathbf{z}_{t_0:t-1}$), we define four configurations based on how the context embedding is computed:

1. INUN: Only the historical inundation ($k\mathbf{x}_{t_0:t-1}^0$) used.
2. INUN, ELEV: We use historical inundation data $k\mathbf{x}_{t_0:t-1}^0$ and the elevation matrix $k\mathbf{s}$.
3. INUN, COV: We use historical inundation data $k\mathbf{x}_{t_0:t-1}^0$ and the temporal covariates $\mathbf{z}_{t_0:t-1}$.
4. INUN, ELEV, COV: We include all three components.

We ran five experiment runs for each configuration, where we trained and tested DIFF-FLOOD on the Tidewatch dataset with $K = 10$ and $D = 64$. Figure 4 shows the performance of the four configurations in terms of NACRPS and NRMSE. We observe that, configuration (INUN, COV) and (INUN, ELEV) are both better than the configuration (INUN) in terms of the two metrics. This implies that DIFF-FLOOD is able to utilize both elevation and temporal covariates as context effectively. We also observe that, including the temporal covariates results in a greater improvement (43%, 41% improvement over INUN in terms of NACRPS and NRMSE, respectively) than including spatial context (8%, 4%). However, best performance is achieved when both are utilized (48%, 47% improvement over INUN).

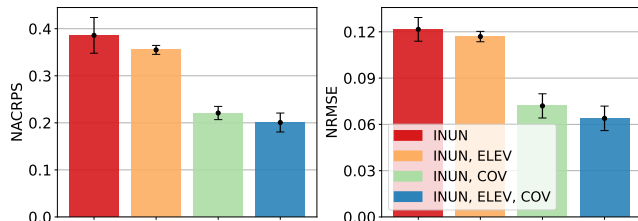


Figure 4: Bar-plots showing performance comparison of the four configurations of DIFF-FLOOD on our test dataset of configuration $64 \times 64 \times 10$, in terms of two metrics. The height of the bars represent mean of the metric and the vertical black lines represent standard deviation. Lower metric value is better. Our proposed architecture of DIFF-FLOOD is able to utilize elevation (ELEV) and temporal covariates (COV) individually, resulting in improved performance in terms of both of our two metrics. Best performance is achieved when both are used.



Figure 5: **(left)** A school area in the Eastern Shore of Virginia. The red cells and four orange patches overlap with the school area. A possible query is: what is the probability that the flooding level in the school area will be above d units within next T hours? **(right)** A route coming out from the school. The red cells and the eight orange patches overlap with the route. A possible query is: what is the probability that the route coming out of the school will not be flooded in the next T hours?

7 Discussion and Conclusion

Once DIFF-FLOOD is trained, we can use it to answer inundation-scenario related queries relevant to policymakers. Example queries are as follows:

- **Query 1:** *What is the probability that the flooding level in an area A will be above d units within next T hours?* (Figure 5, left)
- **Query 2:** *Given a route, what is the probability that the route will not be flooded in the next T hours?* (Figure 5, right)

Such queries are of special interest to city officials; answer to these queries will help to better prepare and respond to emergencies. The key idea for answering such queries is that, we have a sampling method in the form a trained DIFF-FLOOD model and we can use it to sample inundation scenarios from the distribution of possible scenarios. We use the sampled scenarios to calculate our desired probability value. In the supplementary materials, we provide a detailed algorithm for answering such queries using a trained DIFF-FLOOD model.

Although DIFF-FLOOD is developed to solve the task of coastal inundation forecasting, it is generalizable enough to be extended to other spatiotemporal forecasting tasks (e.g., occupancy detection, traffic forecasting). DIFF-FLOOD supports conditioning on time-invariant spatial features, as well as, on temporal co-variates. In our future work, we plan to evaluate its performance in diverse spatiotemporal forecasting tasks.

To conclude, we have presented a probabilistic spatiotemporal forecasting method, DIFF-FLOOD that takes both spatial and temporal context into account during its training and forecasting phase. We have performed a case study on the coastal inundation forecasting task for the Eastern Shore of Virginia. Through our experiments, we show that DIFF-FLOOD outperforms existing forecasting methods in predicting coastal inundation. Additionally, the architecture of DIFF-FLOOD allows it to scale to large forecasting tasks at fine spatial resolution, compared to current methods.

A Extended Related Work

Hydrology Models Traditionally, inundation has been simulated through hydro-dynamical physics-based 1D/2D dual drainage models. By simulating water flow in water bodies and coupling them with 1D or 2D hydrodynamic models, these models can predict inundation in surfaces. For example, the 2D model SOBEK [Deltares, 2014] consists of a 1D network with information about the initial water volume of rivers and 2D rectangular computational cells. By coupling these two parts, the model uses the Saint-Venant flow equation and 2D shallow water equation to calculate discharge between cells and determine the water level at each cell of the Digital Elevation Model (DEM). TELEMAC-2D [Vu *et al.*, 2015] also solves 2D shallow water equation to simulate water flow. However, its primary purpose is to understand flow through water bodies. Therefore, this makes this model more suitable for coastal regions, contrary to SOBEK which is more suitable for urban areas. Polymorphic models like SCHISM [Zhang *et al.*, 2016] can capture water flow at very high resolution, down to even a few meters due to their hybrid gridding system and localized coordinate system. Despite these models’ ability to model inundation accurately at fine resolution, the computation time associated with them makes them infeasible for real-time forecasting.

Regression-based Models Early approaches in finding surrogates for hydrology models involved applying various regression-based methods. [Chang *et al.*, 2010] first applied K-means clustering to pre-process data to find inundation control points. The authors then applied linear regression or neural networks to predict inundation for grids depending on whether they are linearly correlated with the control points or not. [Bermúdez *et al.*, 2019] explored non-parametric regression approach based on least square support vector machine (SVM) as surrogate for 2D hydrodynamic models. [Lee and Kim, 2021] created an offline rainfall-runoff-inundation database by simulating hydrology models over multiple scenarios. Then, they trained a logistic regression-based approach based on the database to estimate the parameters to predict the risk of flooding for each region. Their goal was then to use the trained regressor to generate near real-time prediction of inundation probability given the runoff to the grid from simulated and realistic rainfall scenario.

Deep Learning (DL) Models Many DL models have been explored as possible surrogates for Physics Based Models (PBM). One research work [Pan *et al.*, 2011] applied a combined approach consisting of principal component analysis (PCA) and a feed-forward neural network. Their approach involved inundation prediction at various locations in the next timestep by looking at a fixed window of rainfall history of N different rainfall gauges. First, they applied PCA on these various rainfall gauge histories to reduce the dimensionality before using them as input to the feed-forward neural network. Since such neural networks are expected to fail where data availability is limited, another work [Xie *et al.*, 2021] explored the potential of a hybrid feed-forward neural network-based approach where they used two block-based neural networks along with the traditional point-based neural network and found superiority of the hybrid approach over other in

the data-sparse region. Consequently, convolutional neural network (CNN) was explored [Kabir *et al.*, 2020] as a potential surrogate. After their model was trained to predict the output simulated from a 2D hydrology model, they used it to simulate two real-event flood scenarios in a region of UK. Since these models are not able to capture long-term temporal dependencies, researchers have recently explored [Roy *et al.*, 2023] seq2seq LSTM model as surrogates to hydrology models. Such model was also applied in forecasting for multi-step future horizons.

Diffusion Model TimeGrad [Rasul *et al.*, 2021] was the pioneering work that proposed the use of diffusion models for time-series forecasting tasks. They used temporal covariates and embedded historical data as conditions for the diffusion model to denoise the prediction for the next time step. CSDI Tashiro *et al.* [2021] does the same but instead of encoding with a Recurrent Neural Network (RNN) as done in TimeGrad, they leverage a transformer-based architecture. SSSD^{S4} Alcaraz and Strodtzoff [2022] uses a S4 model Gu *et al.* [2021] to capture the encoding which is particularly useful in capturing long-term dependencies. Also, instead of performing diffusion along both temporal and input channel dimensions, they perform diffusion only along the temporal dimension. Different from these, D^3 VAE [Li *et al.*, 2022] uses coupled diffusion process and bidirectional variational autoencoder to better forecast in longer horizon and improve interpretability. The State-of-the-Art Diffusion-based model DiffSTG [Wen *et al.*, 2023] devised a modified architecture for the reverse process of diffusion model combining UNet and GNN to capture temporal and spatial dependencies, respectively. However, both these methods scale poorly with the growth in number of variables.

B Denoising Diffusion Model

In this section, we provide an overview of denoising diffusion models.

Let $\mathbf{x}^0 \sim q_\chi(\mathbf{x}^0)$ denote the multivariate training vector from some input space $\chi = \mathbb{R}^D$ and true distribution $q_\chi(\mathbf{x}^0)$. In diffusion probabilistic models, we aim to approximate $q_\chi(\mathbf{x}^0)$ by a probability density function $p_\theta(\mathbf{x}^0)$ where θ denotes the set of trainable parameters. Diffusion probabilistic models Sohl-Dickstein *et al.* [2015]; Luo [2022] are a special class of Hierarchical Variational Autoencoders Kingma *et al.* [2016]; Sørensen *et al.* [2016] with the form $p_\theta(\mathbf{x}^0) = \int p_\theta(\mathbf{x}^{0:N}) d\mathbf{x}^{1:N}$; here $\mathbf{x}^1, \mathbf{x}^2, \dots, \mathbf{x}^N$ are latent variables. Three key properties of diffusion models are: (i) all of the latent variables are assumed to have the dimension D as \mathbf{x}^0 , (ii) the approximate posterior $q(\mathbf{x}^{1:N}|\mathbf{x}^0)$,

$$q(\mathbf{x}^{1:N}|\mathbf{x}^0) = \prod_{n=1}^N q(\mathbf{x}^n|\mathbf{x}^{n-1})$$

is fixed to a Markov chain (often referred to as the *forward* process), and (iii) the structure of the latent encoder at each hierarchical step is pre-defined as a linear Gaussian model as follows:

$$q(\mathbf{x}^n|\mathbf{x}^{n-1}) = \mathcal{N}(\mathbf{x}^n; \sqrt{1 - \beta_n}\mathbf{x}^{n-1}, \beta_n\mathbf{I}).$$

Additionally, the Gaussian parameters $(\beta_1, \beta_2, \dots, \beta_n)$ are chosen in such a way that we have: $q(\mathbf{x}^N) = \mathcal{N}(\mathbf{x}^N; \mathbf{0}, \mathbf{I})$.

The joint distribution $p_\theta(\mathbf{x}^{0:N})$ is called the reverse process. It is defined as a Markov chain with learned Gaussian transitions beginning at $p(\mathbf{x}^N)$.

$$p_\theta(\mathbf{x}^{0:N}) = p(\mathbf{x}^N) \prod_{n=1}^N p_\theta(\mathbf{x}^{n-1}|\mathbf{x}^n).$$

Each subsequent transition is parameterized as follows:

$$p_\theta(\mathbf{x}^{n-1}|\mathbf{x}^n) = \mathcal{N}(\mathbf{x}^{n-1}; \mu_\theta(\mathbf{x}^n, n), \Sigma_\theta(\mathbf{x}^n, n)\mathbf{I}) \quad (20)$$

Both $\mu_\theta : \mathbb{R}^D \times \mathbb{N} \rightarrow \mathbb{R}^D$ and $\Sigma_\theta : \mathbb{R}^D \times \mathbb{N} \rightarrow \mathbb{R}^+$ take two inputs: $\mathbf{x}^n \in \mathbb{R}^D$ and the noise step $n \in \mathbb{N}$. The parameters θ are learned by fitting the model to the data distribution $q_\chi(\mathbf{x}^0)$. This is done by minimizing the negative log-likelihood via a variational bound:

$$\begin{aligned} \log p_\theta(\mathbf{x}^0) &= \log \int p_\theta(\mathbf{x}^{0:N}) d\mathbf{x}^{1:N} \\ &= \log \mathbb{E}_{q(\mathbf{x}^{1:N}|\mathbf{x}^0)} \frac{p_\theta(\mathbf{x}^{0:N})}{q(\mathbf{x}^{1:N}|\mathbf{x}^0)} \\ &\geq \mathbb{E}_{q(\mathbf{x}^{1:N}|\mathbf{x}^0)} \log \frac{p_\theta(\mathbf{x}^{0:N})}{q(\mathbf{x}^{1:N}|\mathbf{x}^0)} \end{aligned} \quad (21)$$

$$\implies -\log p_\theta(\mathbf{x}^0) \leq \mathbb{E}_{q(\mathbf{x}^{1:N}|\mathbf{x}^0)} \log \frac{q(\mathbf{x}^{1:N}|\mathbf{x}^0)}{p_\theta(\mathbf{x}^{0:N})} \quad (22)$$

Here, we get (21) by applying Jensen's inequality. We indirectly minimize the negative log-likelihood of the data, i.e., $-\log p_\theta(\mathbf{x}^0)$, by minimizing the right hand side of (22). We can show that it is equal to:

$$\mathbb{E}_{q(\mathbf{x}^{1:N}|\mathbf{x}^0)} \left[-\log p_\theta(\mathbf{x}^N) + \sum_{n=1}^N \log \frac{q(\mathbf{x}^n|\mathbf{x}^{n-1})}{p_\theta(\mathbf{x}^{n-1}|\mathbf{x}^n)} \right] \quad (23)$$

Ho *et al.* [2020] showed that the forward process has the following property: we can sample \mathbf{x}^n using \mathbf{x}^0 at any noise step n in closed form. Let, $\alpha_n = 1 - \beta_n$, and $\bar{\alpha}_n = \prod_{i=1}^n \alpha_i$. Then, we have:

$$q(\mathbf{x}^n|\mathbf{x}^0) = \mathcal{N}(\mathbf{x}^n; \sqrt{\bar{\alpha}_n}\mathbf{x}^0, (1 - \bar{\alpha}_n)\mathbf{I}). \quad (24)$$

The authors then showed that (23) can be written as KL-divergence between Gaussian distributions:

$$\begin{aligned} &-\mathbb{E}_{q(\mathbf{x}^1|\mathbf{x}^0)} \log p_\theta(\mathbf{x}^0|\mathbf{x}^1) + D_{KL}(q(\mathbf{x}^N|\mathbf{x}^0) || p_\theta(\mathbf{x}^N)) \\ &+ \sum_{n=2}^N \mathbb{E}_{q(\mathbf{x}^n|\mathbf{x}^0)} [D_{KL}(q(\mathbf{x}^{n-1}|\mathbf{x}^n, \mathbf{x}^0) || p_\theta(\mathbf{x}^{n-1}|\mathbf{x}^n))] \end{aligned} \quad (25)$$

Here, the authors conditioned the forward process posterior on \mathbf{x}^0 , i.e. $q(\mathbf{x}^{n-1}|\mathbf{x}^n, \mathbf{x}^0)$, because then it becomes tractable as follows:

$$q(\mathbf{x}^{n-1}|\mathbf{x}^n, \mathbf{x}^0) = \mathcal{N}(\mathbf{x}^{n-1}; \tilde{\mu}_n(\mathbf{x}^n, \mathbf{x}^0), \tilde{\beta}_n\mathbf{I}) \quad (26)$$

where,

$$\tilde{\mu}_n(\mathbf{x}^n, \mathbf{x}^0) = \frac{\sqrt{\bar{\alpha}_n}(1 - \bar{\alpha}_{n-1})}{1 - \bar{\alpha}_n}\mathbf{x}^n + \frac{\sqrt{\bar{\alpha}_{n-1}}(1 - \alpha_n)}{1 - \bar{\alpha}_n}\mathbf{x}^0 \quad (27)$$

$$\tilde{\beta}_n = \frac{1 - \bar{\alpha}_{n-1}}{1 - \bar{\alpha}_n}\beta_n \quad (28)$$

Since, the forward process posterior (26) and the backward transition (20) are both Gaussian, we can write the KL-divergence between them as follows:

$$\begin{aligned} D_{KL}(q(\mathbf{x}^{n-1}|\mathbf{x}^n, \mathbf{x}^0) || p_\theta(\mathbf{x}^{n-1}|\mathbf{x}^n)) \\ = \frac{1}{2\tilde{\beta}_n} \|\tilde{\mu}_n(\mathbf{x}^n, \mathbf{x}^0) - \mu_\theta(\mathbf{x}^n, n)\|_2^2 + C \end{aligned} \quad (29)$$

Here, C is a constant independent of θ , and we assume that

$$\Sigma_\theta = \tilde{\beta}_n = \frac{1 - \bar{\alpha}_{n-1}}{1 - \bar{\alpha}_n}\beta_n \quad (30)$$

As $\mu_\theta(\mathbf{x}^n, n)$ is conditioned on \mathbf{x}^n , similar to $\tilde{\mu}_n(\mathbf{x}^n, \mathbf{x}^0)$ in (27), we can give it the form:

$$\mu_\theta(\mathbf{x}^n, n) = \frac{\sqrt{\bar{\alpha}_n}(1 - \bar{\alpha}_{n-1})}{1 - \bar{\alpha}_n}\mathbf{x}^n + \frac{\sqrt{\bar{\alpha}_{n-1}}\beta_n}{1 - \bar{\alpha}_n}\hat{\mathbf{x}}_\theta(\mathbf{x}^n, n) \quad (31)$$

Here, $\hat{\mathbf{x}}_\theta(\mathbf{x}^n, n)$ is a neural network that predicts \mathbf{x}^0 from noisy vector \mathbf{x}^n and noise step n . With this parameterization, we can show that:

$$\begin{aligned} D_{KL}(q(\mathbf{x}^{n-1}|\mathbf{x}^n, \mathbf{x}^0) || p_\theta(\mathbf{x}^{n-1}|\mathbf{x}^n)) \\ = \frac{1}{2\tilde{\beta}_n} \frac{\bar{\alpha}_{n-1}\beta_n^2}{(1 - \bar{\alpha}_n)^2} \|\mathbf{x}^0 - \hat{\mathbf{x}}_\theta(\mathbf{x}^n, n)\|_2^2 \end{aligned} \quad (32)$$

Therefore, optimizing a diffusion model can be done by training a neural network to predict the original ground truth vector from an arbitrarily noisy version of it. To approximately minimize the summation term in the objective (25) across all noise steps n , we can minimize the expectation over all noise steps as follows:

$$\operatorname{argmin}_\theta \mathbb{E}_{n \sim U[2, N]} \mathbb{E}_{q(\mathbf{x}^n|\mathbf{x}^0)} \frac{1}{2\tilde{\beta}_n} \frac{\bar{\alpha}_{n-1}\beta_n^2}{(1 - \bar{\alpha}_n)^2} \|\mathbf{x}^0 - \hat{\mathbf{x}}_\theta(\mathbf{x}^n, n)\|_2^2 \quad (33)$$

This can be done by using stochastic samples over noise steps. Once trained, to sample from the reverse process $\mathbf{x}^{n-1} \sim p_\theta(\mathbf{x}^{n-1}|\mathbf{x}^n)$, we first sample \mathbf{x}^N from $\mathcal{N}(\mathbf{0}, \mathbf{I})$. Then, we compute:

$$\mathbf{x}^{n-1} = \mu_\theta(\mathbf{x}^n, n) + \sqrt{\Sigma_\theta} \mathbf{v} \quad (34)$$

Here, $\mathbf{v} \sim \mathcal{N}(\mathbf{0}, \mathbf{I})$ for $n \in [2, N]$ and $\mathbf{v} = \mathbf{0}$ when $n = 1$. $\mu_\theta(\mathbf{x}^n, n)$ and Σ_θ are computed using (31) and (30), respectively.

C Inundation Scenario Queries

Once DIFF-FLOOD is trained, we can use it to answer inundation scenario-based queries relevant to policymakers. In this Section, we discuss a few of such queries.

• **Query 1:** *What is the probability that the flooding level in an area A will be above d units within next T hours?*

We use Algorithm 3 as a sub-routine to answer this query. First, we identify the cells that overlap with A (red cells in Figure 6 left). Let C_A denote the set of these cells. If at least one cell $c \in C_A$ has a flooding level above d units in

Algorithm 3: Calculate the probability that the flooding level in an area A will be $\leq d$ units in the next T hours.

Input: Query area A as a Polygon, Flooding level threshold d , Prediction Length T , Trained DIFF-FLOOD Model.

- 1 $C_A \leftarrow$ Set of grid cells that overlap with A .
 - 2 $\mathcal{P}_A \leftarrow$ Set of patches where each patch $P \in \mathcal{P}_A$ contains at-least one cell $c \in C_A$.
 - 3 **for** each patch $P \in \mathcal{P}_A$ **do**
 - 4 Generate M samples for patch P with prediction length T (using Algorithm 2 in main paper).
 - 5 $num_scenarios(P_{\leq d}) \leftarrow$ Number of samples where each cell $c \in P \cap C_A$ has flooding level $\leq d$.
 - 6 $probability(P_{\leq d}) \leftarrow num_scenarios(P_{\leq d})/M$
 - 7 $p \leftarrow \prod_{P \in \mathcal{P}_A} probability(P_{\leq d})$
 - 8 **return** p .
-

the next T hours, we say area A has a flooding level above d units.

In Algorithm 3 line 2, we identify the patches that contain at-least one cell $c \in C_A$ (four orange patches in Figure 6, **left**). Let the set of such patches be denoted by \mathcal{P}_A . For each patch $P \in \mathcal{P}_A$, we generate M number of samples (using Algorithm 2 in main paper) with prediction length of T hours (line 4). Then, we calculate the number of samples where all cells $c \in P \cap C_A$ have a inundation level $\leq d$ units (line 5). We denote it by $num_scenarios(P_{\leq d})$. Subsequently, we calculate the probability that all the cells $c \in P \cap C_A$ have flooding level $\leq d$ units to be $probability(P_{\leq d}) = num_scenarios(P_{\leq d})/M$ (line 6). We assume the inundation levels in different patches to be independent. Therefore, the probability that all cells $c \in C_A$ have flooding level $\leq d$ units is calculated to be $p = \prod_{P \in \mathcal{P}_A} probability(P_{\leq d})$ (line 7).



Figure 6: **(left)** A school area in the Eastern Shore of Virginia. The red cells and four orange patches overlap with the school area. A possible query is: what is the probability that the flooding level in the school area will be above d units within next T hours? **(right)** A route coming out from the school. The red cells and the eight orange patches overlap with the route. A possible query is: what is the probability that the route coming out of the school will not be flooded in the next T hours?

Since we require the probability of flooding level being **above** d units in area A , our desired probability value is $(1 - p)$.

- **Query 2:** Given an evacuation route, what is the probability that the route will not be flooded in the next T hours? An evacuation route is a sequence of roads that are used for evacuating out of an area. We represent each road using a polygon. Then, a route is also a polygon, which is the union of all of its member road polygons. Let the route polygon be denoted by A . Then, we use Algorithm 3 with $d = 0$, to calculate our desired probability value.

It is important to note that, we can have more complex queries. For instance, a more refined version of Query 1 can be: *what is the probability that at-least half of the region A will have flooding level above d units in the next T hours?* The key idea for answering such queries is that, we have a sampling method in the form a trained DIFF-FLOOD model and we can use it to sample inundation scenarios from the distribution of possible scenarios. We use the sampled scenarios to calculate our desired probability value.

D Hyper-parameters

Hyper-parameter	Value
Learning rate	0.001
Learning rate update step size	5 epochs
Learning rate update factor	0.5
Number of epochs	30
Training batch size	32
Validation and test batch size	4
Context length	12 timesteps
Training prediction length	1 timestep
Validation and test prediction length	12 timesteps
Number of diffusion steps	20
Diffusion β_{min}	10^{-4}
Diffusion β_{max}	1
NO. of scenarios generated for validation	2
NO. of scenarios generated for test	8

Table 2: Shared hyper-parameters for all of our patch configurations in Table 1 of main paper.

E Patch Visualization

Hyper-parameter	$D = 16$	$D = 64$	$D = 80$	$D = 96$
Number of Convolution Blocks	1	3	3	3
Convolution block number of Channels	[8]	[16, 32, 64]	[16, 32, 64]	[16, 32, 64]
Context embedding dimension	32	32	64	96
UNet Number of Down (and Up) blocks	4	4	4	4
Number of ResNet layers per UNet block	2	2	2	2
UNet Down Blocks: Number of Channels	[8, 16, 32, 32]	[16, 32, 32, 64]	[16, 32, 32, 64]	[16, 32, 32, 64]
UNet Number of Cross-attention Down / Up Blocks	2	2	2	2
Group Normalization: Number of Groups	8	8	8	8

Table 3: Hyper-parameters for different patch configurations

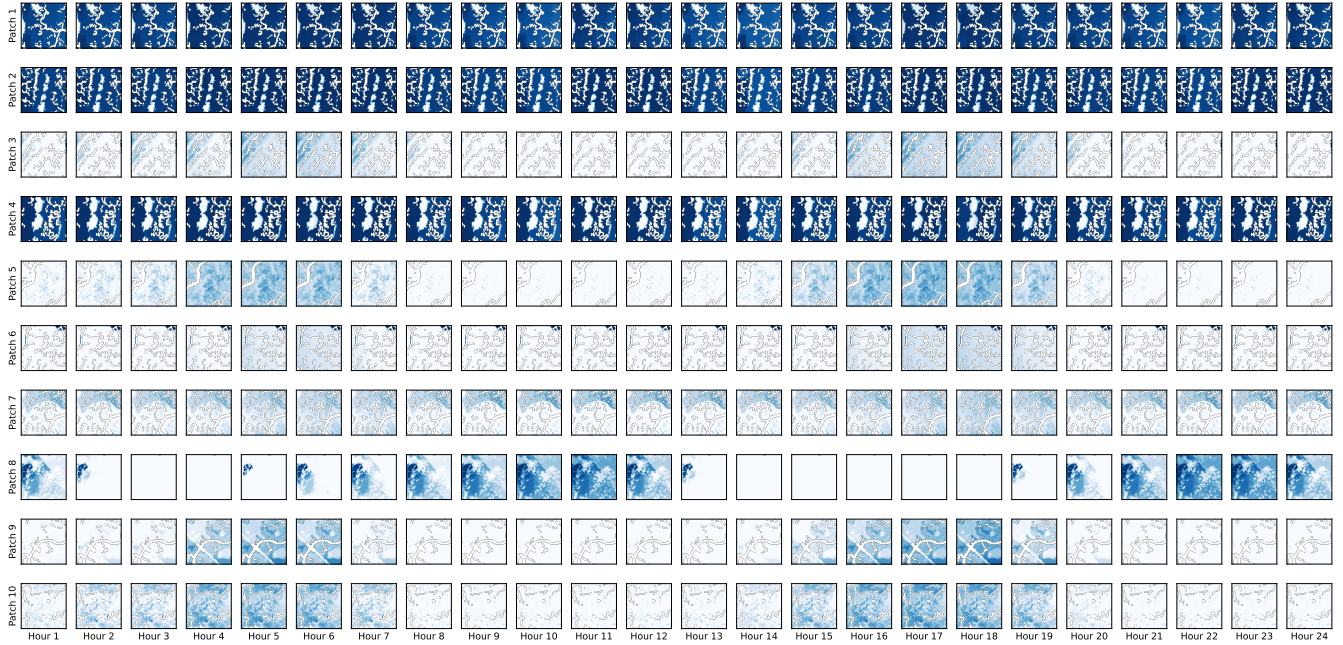


Figure 7: Visualization of inundation on 10, 64×64 patches in the first 24 hours of training data. The darker the shade of blue, the higher the inundation value.

References

Farzana Yasmin Ahmad et al. A comprehensive evaluation of generative models in calorimeter shower simulation. *arXiv preprint arXiv:2406.12898*, 2024.

Juan Miguel Lopez Alcaraz and Nils Strodthoff. Diffusion-based time series imputation and forecasting with structured state space models. *arXiv preprint arXiv:2208.09399*, 2022.

Oz Amram and Kevin Pedro. Denoising diffusion models

with geometry adaptation for high fidelity calorimeter simulation. *Physical Review D*, 108(7):072014, 2023.

Jacob Austin, Daniel D Johnson, Jonathan Ho, Daniel Tarlow, and Rianne Van Den Berg. Structured denoising diffusion models in discrete state-spaces. *Advances in Neural Information Processing Systems*, 34:17981–17993, 2021.

María Bermúdez, Luis Cea, and Jerónimo Puertas. A rapid flood inundation model for hazard mapping based on least

- squares support vector machine regression. *Journal of Flood Risk Management*, 12:e12522, 2019.
- Marin Biloš, Kashif Rasul, Anderson Schneider, Yuriy Nevmyvaka, and Stephan Günnemann. Modeling temporal data as continuous functions with stochastic process diffusion. In *International Conference on Machine Learning*, pages 2452–2470. PMLR, 2023.
- Li-Chiu Chang, Hung-Yu Shen, Yi-Fung Wang, Jing-Yu Huang, and Yen-Tso Lin. Clustering-based hybrid inundation model for forecasting flood inundation depths. *Journal of hydrology*, 385(1-4):257–268, 2010.
- Ping Chang, Huayu Li, Stuart F. Quan, Shuyang Lu, Shu-Fen Wung, Janet Roveda, and Ao Li. A transformer-based diffusion probabilistic model for heart rate and blood pressure forecasting in intensive care unit. *Computer Methods and Programs in Biomedicine*, 246:108060, April 2024.
- Deltares. Sobek—hydrodynamics, rainfall runoff and real time control. 2014.
- Prafulla Dhariwal and Alexander Nichol. Diffusion models beat gans on image synthesis. *Advances in neural information processing systems*, 34:8780–8794, 2021.
- Tal Ezer and Larry P Atkinson. Accelerated flooding along the us east coast: On the impact of sea-level rise, tides, storms, the gulf stream, and the north atlantic oscillations. *Earth’s Future*, 2(8):362–382, 2014.
- Tal Ezer. Analysis of the changing patterns of seasonal flooding along the us east coast. *Ocean Dynamics*, 70(2):241–255, 2020.
- Albert Gu, Karan Goel, and Christopher Ré. Efficiently modeling long sequences with structured state spaces. *arXiv preprint arXiv:2111.00396*, 2021.
- Kaihua Guo et al. Urban surface water flood modelling—a comprehensive review of current models and future challenges. *Hydrology and Earth System Sciences*, 25(5):2843–2860, 2021.
- Jonathan Ho, Ajay Jain, and Pieter Abbeel. Denoising diffusion probabilistic models. *Advances in neural information processing systems*, 33:6840–6851, 2020.
- Jennifer M Jacobs, Lia R Cattaneo, William Sweet, and Theodore Mansfield. Recent and future outlooks for nuisance flooding impacts on roadways on the us east coast. *Transportation research record*, 2672(2):1–10, 2018.
- Syed Kabir, Sandhya Patidar, Xilin Xia, Qihua Liang, Jeffrey Neal, and Gareth Pender. A deep convolutional neural network model for rapid prediction of fluvial flood inundation. *Journal of Hydrology*, 590:125481, 2020.
- Durk P Kingma, Tim Salimans, Rafal Jozefowicz, Xi Chen, Ilya Sutskever, and Max Welling. Improved variational inference with inverse autoregressive flow. *Advances in neural information processing systems*, 29, 2016.
- Guokun Lai, Wei-Cheng Chang, Yiming Yang, and Hanxiao Liu. Modeling long-and short-term temporal patterns with deep neural networks. In *The 41st international ACM SIGIR conference on research & development in information retrieval*, pages 95–104, 2018.
- Jaeyeong Lee and Byunghyun Kim. Scenario-based real-time flood prediction with logistic regression. *Water*, 13(9):1191, 2021.
- Yaguang Li, Rose Yu, Cyrus Shahabi, and Yan Liu. Diffusion convolutional recurrent neural network: Data-driven traffic forecasting. *arXiv preprint arXiv:1707.01926*, 2017.
- Yan Li, Xinjiang Lu, Yaqing Wang, and Dejing Dou. Generative time series forecasting with diffusion, denoise, and disentanglement. *Advances in Neural Information Processing Systems*, 35:23009–23022, 2022.
- Jon Derek Loftis, Molly Mitchell, Daniel Schatt, David R. Forrest, Harry V. Wang, David Mayfield, and William A. Stiles. Validating an operational flood forecast model using citizen science in hampton roads, va, usa. *Journal of Marine Science and Engineering*, 7(8):242, July 2019.
- Jon Derek Loftis. Exploring latent verification methods for inundation forecasting models through remote sensing networks and community science. In *OCEANS 2022, Hampton Roads*. IEEE, October 2022.
- Calvin Luo. Understanding diffusion models: A unified perspective. *arXiv preprint arXiv:2208.11970*, 2022.
- OpenTopography. Usgs 1/3 arc-second digital elevation models, 2021.
- T-Y Pan, J-S Lai, T-J Chang, H-K Chang, K-C Chang, and Y-C Tan. Hybrid neural networks in rainfall-inundation forecasting based on a synthetic potential inundation database. *Natural Hazards and Earth System Sciences*, 11(3):771–787, 2011.
- Aditya Ramesh, Prafulla Dhariwal, Alex Nichol, Casey Chu, and Mark Chen. Hierarchical text-conditional image generation with clip latents. *arXiv preprint arXiv:2204.06125*, 1(2):3, 2022.
- Kashif Rasul, Calvin Seward, Ingmar Schuster, and Roland Vollgraf. Autoregressive denoising diffusion models for multivariate probabilistic time series forecasting. In *International Conference on Machine Learning*, pages 8857–8868. PMLR, 2021.
- Robin Rombach, Andreas Blattmann, Dominik Lorenz, Patrick Esser, and Björn Ommer. High-resolution image synthesis with latent diffusion models. In *Proceedings of the IEEE/CVF Conference on Computer Vision and Pattern Recognition (CVPR)*, pages 10684–10695, June 2022.
- Binata Roy, Jonathan L Goodall, Diana McSpadden, Steven Goldenberg, and Malachi Schram. Application of lstm and seq2seq lstm surrogate models for forecasting multi-step-ahead nuisance flooding of flood-vulnerable streets in norfolk, virginia. In *AGU Fall Meeting Abstracts*, volume 2023, pages H41V–02, 2023.
- David Salinas, Michael Bohlke-Schneider, Laurent Callot, Roberto Medico, and Jan Gasthaus. High-dimensional multivariate forecasting with low-rank gaussian copula processes. *Advances in neural information processing systems*, 32, 2019.
- Janascha Sohl-Dickstein, Eric Weiss, Niru Maheswaranathan, and Surya Ganguli. Deep unsupervised learning using

- nonequilibrium thermodynamics. In *International conference on machine learning*, pages 2256–2265. PMLR, 2015.
- Casper Kaae Sønderby, Tapani Raiko, Lars Maaløe, Søren Kaae Sønderby, and Ole Winther. Ladder variational autoencoders. *Advances in neural information processing systems*, 29, 2016.
- DL Swain, Oliver EJ Wing, Paul D Bates, JM Done, KA Johnson, and DR Cameron. Increased flood exposure due to climate change and population growth in the united states. *Earth's Future*, 8(11):e2020EF001778, 2020.
- WJ Syme. TufLOW-two & onedimensional unsteady flow software for rivers, estuaries and coastal waters. In *IEAust Water Panel Seminar and Workshop on 2d Flood Modelling, Sydney*, 2001.
- Yusuke Tashiro, Jiaming Song, Yang Song, and Stefano Ermon. CSDI: Conditional score-based diffusion models for probabilistic time series imputation. *Advances in Neural Information Processing Systems*, 34:24804–24816, 2021.
- Tidewatch. Tidewatch maps, 2025. <https://cmap2.vims.edu/SCHISM/TidewatchViewer.html>, 2025.
- Tung T Vu, Phuoc KT Nguyen, Lloyd HC Chua, and Adrian WK Law. Two-dimensional hydrodynamic modelling of flood inundation for a part of the mekong river with teleMAC-2d. *British Journal of Environment and Climate Change*, 5(2):162–175, 2015.
- Haomin Wen, Youfang Lin, Yutong Xia, Huaiyu Wan, Qingsong Wen, Roger Zimmermann, and Yuxuan Liang. DiffSTG: Probabilistic spatio-temporal graph forecasting with denoising diffusion models. In *Proceedings of the 31st ACM International Conference on Advances in Geographic Information Systems*, pages 1–12, 2023.
- Robert L Winkler, Javier Munoz, José L Cervera, José M Bernardo, Gail Blattenberger, Joseph B Kadane, Dennis V Lindley, Allan H Murphy, Robert M Oliver, and David Ríos-Insua. Scoring rules and the evaluation of probabilities. *Test*, 5:1–60, 1996.
- Donald Wuebbles, David Fahey, Eugene Takle, Kathy Hubbard, Jeff Arnold, Benjamin DeAngelo, Sarah Doherty, David Easterling, James Edmonds, Timothy Edmonds, et al. Climate science special report: Fourth national climate assessment (nca4), volume i. 2017.
- Shuai Xie, Wenyan Wu, Sebastian Mooser, QJ Wang, Rory Nathan, and Yuefei Huang. Artificial neural network based hybrid modeling approach for flood inundation modeling. *Journal of Hydrology*, 592:125605, 2021.
- Kun Yang, Rachel A Davidson, Humberto Vergara, Randall L Kolar, Kendra M Dresback, Brian A Colle, Brian Blanton, Tricia Wachtendorf, Jennifer Trivedi, and Linda K Nozick. Incorporating inland flooding into hurricane evacuation decision support modeling. *Natural Hazards*, 96:857–878, 2019.
- Dongchao Yang, Jianwei Yu, Helin Wang, Wen Wang, Chao Weng, Yuexian Zou, and Dong Yu. DiffSound: Discrete diffusion model for text-to-sound generation. *IEEE/ACM Transactions on Audio, Speech, and Language Processing*, 31:1720–1733, 2023.
- Ruihan Yang, Prakhar Srivastava, and Stephan Mandt. Diffusion probabilistic modeling for video generation. *Entropy*, 25(10):1469, 2023.
- Faria T Zahura and Jonathan L Goodall. Predicting combined tidal and pluvial flood inundation using a machine learning surrogate model. *Journal of Hydrology: Regional Studies*, 41:101087, 2022.
- ADL Zanchetta and P Coulibaly. Hybrid surrogate model for timely prediction of flash flood inundation maps caused by rapid river overflow, forecasting, 4, 126–148, 2022.
- Lvmin Zhang et al. Adding conditional control to text-to-image diffusion models. In *Proceedings of the IEEE/CVF International Conference on Computer Vision*, pages 3836–3847, 2023.
- Yinglong J Zhang, Fei Ye, Emil V Stanev, and Sebastian Grashorn. Seamless cross-scale modeling with schism. *Ocean Modelling*, 102:64–81, 2016.